

River ecomorphodynamic models exhibit features of nonlinear dynamics and chaos

I. Cunico¹, W. Bertoldi¹, F. Caponi², H. A. Dijkstra³, A. Sivilgia¹

¹Department of Civil, Environmental and Mechanical Engineering, University of Trento, Italy

²Laboratory of Hydraulics, Hydrology and Glaciology (VAW), ETH Zurich, Zurich, Switzerland

³Institute for Marine and Atmospheric Research Utrecht, Utrecht University, Utrecht, The Netherlands

Key Points:

- Coevolution of riverbed and vegetation, mediated by intrinsic biogeomorphic feedbacks, exhibits nonlinear dynamics and chaos.
- In our models chaos can occur under a wide range of conditions typical of gravel-bed rivers.
- A zero-dimensional model demonstrates a distinct period-doubling route to chaos.
- The Lyapunov time is short, ranging between 2-4 growth-flood cycles, suggesting a limited predictability horizon for riverbed evolution

Corresponding author: Ilaria Cunico, ilaria.cunico@unitn.it

Abstract

Modeling the nonlinear interactions between flow, sediment, and vegetation is essential for improving our understanding and prediction of river system dynamics. Using simple numerical models, we simulate the key flow-sediment-vegetation interaction where the disturbance is intrinsically generated by the presence of vegetation. In this case, biomass growth modifies the flow field, induces bed scour, and thus potentially causes vegetation uprooting when erosion exceeds root depth. Our results show that this nonlinear feedback produces deterministic chaos under a wide range of conditions, with complex aperiodic dynamics generated by a period-doubling route to chaos. Moreover, our results suggest relatively small values of Lyapunov time, spanning 2-4 growth-flood cycles, which significantly restrict the predictability of riverbed evolution. Although further spatial and temporal processes may add complexity to the system, these results call for the use of ensemble methods and associated uncertainty estimates in ecomorphodynamic models.

Plain Language Summary

Simple models that reproduce the mutual interactions between the physical environment and riparian vegetation show that the evolution of riverbed morphology exhibits chaotic dynamics. This precludes the possibility of predicting long-term riverbed morphology and limits the horizon of predictability, which our analysis estimates to be a few cycles of vegetation growth and removal by floods. These findings have important implications for the management and restoration of river systems, as they suggest that the use of ensemble forecasting methods is necessary to quantify the uncertainty associated with predictions. The nonlinear interaction mechanisms responsible for the chaotic behavior are not limited to rivers and may play a role in other systems where flow disturbance and vegetation resistance are key to their evolution.

1 Introduction

In the last two decades, riparian vegetation has been recognized as one of the fundamental components of river systems, controlling river evolution at different spatial and temporal scales (Corenblit et al., 2007; Gurnell, 2014). Water flow, sediment flux, and vegetation interact through nonlinear processes that control river system dynamics and generate specific biogeomorphic patterns (Murray et al., 2008; Reinhardt et al., 2010; Corenblit et al., 2011; D’Alpaos et al., 2016). At the landscape scale, vegetation establishment has been shown to promote a transition from multi-thread, bar-braided morphologies to single-thread, meandering channels (Tal & Paola, 2007; Braudrick et al., 2009). At the reach scale, biogeomorphic feedbacks support the formation and evolution of islands and secondary channels (Gurnell et al., 2001), control the dynamics of river bars (Bertoldi et al., 2014; Jourdain et al., 2020; Caponi et al., 2020), and play a critical role in shaping river deltaic marshes (Nardin & Edmonds, 2014), facilitating the formation of drainage channel networks in tidal systems (e.g., Temmerman et al., 2007; Schwarz et al., 2018). Interestingly, the effects of these biogeomorphic feedbacks have been shown to be drivers of hysteresis effects (Bau’ et al., 2021) and abrupt shifts (Scheffer et al., 2001; Wang & Temmerman, 2013; Wang et al., 2016), resulting in high sensitivity to rapid forcing and potentially irreversible changes between a state of extensive vegetation encroachment or a completely bare riverbed (e.g., Corenblit et al., 2011; Bertoldi et al., 2014; Bertagni et al., 2018).

Riparian vegetation dynamics are controlled by the balance between vegetation resistance and hydromorphodynamic disturbance, mainly in the form of uprooting by erosion, as this is the only relevant removal mechanism for most fluvial environments (Edmaier et al., 2011; Bywater-Reyes et al., 2015; Bankhead et al., 2017). Bed and bank erosion

can occur regardless of the presence of vegetation, as an external morphological forcing; however, vegetation itself produces changes in the flow field, which can lead to local changes in sediment transport capacity, thereby inducing erosion and deposition patterns. This process generates an intrinsic feedback whereby the presence and growth of vegetation increases the disturbance (e.g., Bouma et al., 2007; Follett & Nepf, 2012; Le Bouteiller & Venditti, 2014) and thus potentially induces vegetation uprooting. This mechanism directly links the presence of vegetation to the magnitude of disturbance, inducing a negative feedback loop whereby greater biomass causes greater disturbance and thus potentially a decrease in biomass (see Fig. 1). This process is common in many fluvial environments where scour occurs in close proximity to individual plants or vegetation patches. Depending on the configuration, scour may occur upstream or laterally of small vegetated patches (e.g., Zong & Nepf, 2012; Kim et al., 2015) or downstream of larger patches covering the entire channel width (e.g., Le Bouteiller & Venditti, 2015; Diehl et al., 2017).

Here we use simplified models that reproduce this main intrinsic interactions between flow, sediment, and vegetation to explore whether vegetated rivers subject to growth and flood disturbance cycles exhibit chaotic behavior and how this affects the predictability horizon of river morphology. The occurrence of chaotic behavior could modify our approach to predictive ecomorphodynamic models, their development, and the interpretation of model results, as has been suggested for other geomorphic systems (Phillips, 2003; Salter et al., 2020). Numerical models are vital for understanding river responses to environmental changes and guiding river management for risk mitigation and ecosystem restoration (Wohl et al., 2015; Palmer & Ruhi, 2019). Understanding biogeomorphic system dynamics is crucial for enhancing ecomorphodynamic model predictions.

2 Modelling Approach

We employed two distinct models with varying levels of complexity to investigate the potential for chaos occurrence and its characterization. First, we used an ecomorphodynamic model (one-dimensional) that explicitly incorporates the spatial distribution of erosion processes and vegetation biomass. It describes temporal changes in riverbed elevation and vegetation abundance along the streamwise direction (Caponi & Siviglia, 2018). The model incorporates a minimal set of biogeomorphic feedbacks that effectively capture the complex interactions between flow, sediment, and vegetation dynamics. Then we simplified the first model by selectively relaxing certain assumptions and removing the spatial component. Both models operate under the key premise that the dynamics of the system are driven by intrinsic feedback mechanisms linking erosion processes, vegetation abundance and mortality (Figure 1).

2.1 One-Dimensional Ecomorphodynamic Model

2.1.1 Hydromorphodynamics

Hydromorphodynamic processes describing the interactions between sediment transport and the flow field are simulated using a one-dimensional approach. The temporal evolution of the riverbed elevation (z_B) is governed by Exner's sediment continuity equation:

$$(1 - p) \frac{\partial z_B}{\partial t} + \frac{\partial q_B}{\partial x} = 0, \quad (1)$$

where p is the sediment porosity and q_B is the unit-width bedload flux in the streamwise direction x . We assume that the flow field adapts instantaneously to the riverbed configuration (Parker, 2004), allowing the water surface elevation to be obtained by numerical integration of the gradually varied flow equation. In this way, we were able to integrate the Exner equation with a much larger time step compared to the fully unsteady model. Importantly, this assumption had no discernible impact on the dynamic behavior of our system, allowing a significant reduction in overall computational time. The global

flow resistance is evaluated using the Manning-Strickler method, where the total shear stress is calculated as $\tau = \rho g u |u| / (ks^2 h^{1/3})$, where ρ is the water density, g is the gravitational acceleration, u is the vertically averaged flow velocity, h is the water depth, $q = uh$ is the unit-width water discharge, and ks is the Strickler coefficient. q_B is evaluated using the Meyer-Peter and Müller formula (Meyer-Peter et al., 1948) as a function of the excess of Shields shear stress θ above a threshold θ_{cr} , where $\theta = \tau / (\rho_s - \rho) g d_s$ and ρ_s and d_s are the sediment density and diameter, respectively. The governing equations are solved numerically by discretizing the numerical domain with uniformly distributed cells (see also Supporting Information Text S1).

2.1.2 Vegetation Dynamics and Biogeomorphic Feedbacks

The equation for vegetation biomass growth in our model is given by the logistic equation, which can be integrated to obtain the following equation:

$$B(t) = \frac{B_0 K e^{\sigma t}}{B_0 (e^{\sigma t} - 1) + K} , \quad (2)$$

where B is the vegetation biomass, B_0 is the initial biomass ($B(t = 0)$), K is the maximum standing biomass (carrying capacity), σ is the vegetation growth rate, and t is time (Supporting Information Fig. S1). To ensure that vegetation grows when starting from a bare riverbed, biomass must be initialized with a small positive value (B_{min}). Biomass increases fluid flow resistance by enhancing local roughness, changing flow patterns, and adding drag (Nepf, 2012). In our model we assume that ks varies linearly with vegetation abundance, changing from ks_g for bare riverbed to ks_v when biomass reaches carrying capacity (Bertoldi et al., 2014; Caponi & Siviglia, 2018). Vegetation also reduces bottom shear stress, affecting sediment transport (Yager & Schmeeckle, 2013; Le Bouteiller & Venditti, 2015). We account for this reduction by multiplying θ by a factor ($\gamma \leq 1$) (Le Bouteiller & Venditti, 2015; Caponi & Siviglia, 2018). We then use the reduced Shields stress ($\gamma\theta$) to calculate the sediment flux (q_B), where the stress reduction coefficient is determined as $\gamma = (ks/ks_g)^2 < 1$. Vegetation uprooting occurs when riverbed erosion exposes a significant proportion of the roots, reducing the anchoring resistance of the plant (Edmaier et al., 2011; Pasquale et al., 2012; Bywater-Reyes et al., 2015). In our model, it occurs when the scour of the riverbed reaches a threshold value ζ_{upr} and is removed on a single cell basis. When vegetation is removed, we set ks to ks_g and B to its minimum value B_{min} . ζ_{upr} does not change during simulations. Importantly, results not reported here show that considering a dynamic rooting depth (i.e. $\zeta_{upr}(t)$) had no impact on the dynamic behavior of our system and thus on the conclusion of this work.

2.1.3 Numerical Simulations

We applied the model to a straight channel with a constant initial slope, in which vegetation can only establish and grow in a limited inner area and occupies the entire width. We chose this configuration to specifically reproduce an erosion process forced only by the presence of vegetation (Le Bouteiller & Venditti, 2014; Caponi & Siviglia, 2018), similarly to the experimental conditions used by Le Bouteiller and Venditti (2014) and Diehl et al. (2017). This choice allows us to isolate the feedback mechanism between vegetation and erosion and thus capture its effects on system dynamics. Although erosion occurs at the downstream boundary in this configuration, it's important to note that the configuration remains applicable regardless of the erosion's location, be it upstream, downstream, or next to small vegetated patches. This setup broadly represents the dynamics at the boundary between vegetated and bare riverbeds, where the presence of biomass intensifies erosion. While other configurations were feasible, our chosen method offers comprehensive control over the erosion process.

The model is forced by alternating sequences of constant discharge floods and periods of low flow during which vegetation grows (growth-flood cycles) (Supporting In-

formation, Fig. S2). We assume that floods repeat deterministically with a fixed period ΔT_F and that the riverbed does not evolve during the low flow periods between two successive floods. Since the duration of vegetation growth (months, years) is much longer than the duration of flood disturbance (hours, days), as is typical for *growth-disturbance* models (Reluga, 2004), we assume that floods occur rapidly and that factors affecting vegetation growth under normal circumstances are temporarily irrelevant during floods (e.g., Bertagni et al., 2018). During floods, the riverbed morphology within the vegetated area adjusts its slope to accommodate the reduced sediment transport capacity due to the presence of vegetation. This leads to erosion and eventually to uprooting (see Supporting Information, Figs. S3A and S3B). The final state of the riverbed after a flood event is influenced by the ratio of disturbance to resistance. A high ratio results in complete uprooting of the vegetation (Supporting Information, Fig. S3C), potentially allowing the riverbed to return to its original configuration, especially if the flood duration is sufficient. Conversely, a lower ratio may result in partial (Supporting Information, Fig. S3D) or no uprooting of vegetation (Supporting Information, Fig. S3E). In these latter scenarios, the slope within the vegetated patch increases. During low flow periods, vegetation grows logistically towards its equilibrium value (carrying capacity K) (Supporting Information, Fig. S1). Vegetation with the highest growth rate, $\sigma = 1$, reaches 99.9% of its maximum growth (i.e. $B/K = 0.999$) at time $t = T_v$. This time scale is used to normalize time as $t^* = t/T_v$. Between two consecutive floods, vegetation that survived to the first flood (B^-) grows reaching a higher biomass (B^+) just before the second flood (Supporting Information, Fig. S2B).

Riverbed-vegetation coevolution is controlled by the balance between hydromorphodynamic disturbance and vegetation resistance (Tal & Paola, 2007). We quantify the magnitude of the erosion process (i.e., a measure of disturbance) by the erosion potential E_p (Caponi & Siviglia, 2018), computed as the mean value of erosion after the first growth-flood cycle, within the vegetated area with biomass at carrying capacity. Vegetation resistance is quantified by its root depth ζ_{upr} . Then, we can define the ratio between disturbance and resistance ($\mathcal{W}_{z_B} = E_p/\zeta_{upr}$) as a normalized parameter to measure the relative strength of the two components, as suggested by previous work (Bertoldi et al., 2014; Caponi & Siviglia, 2018; Perona & Crouzy, 2018). Vegetation establishment is favored by small values of \mathcal{W}_{z_B} . Our numerical model explores various \mathcal{W}_{z_B} values and vegetation growth rates σ maintaining constant flood intervals (ΔT_F). This approach simulates different vegetation types and flood frequencies. Model parameters, typical for gravel-bed rivers, are detailed in Supporting Information Table S1.

2.2 Zero-Dimensional Discrete-Time Growth-Disturbance Model

We developed a conceptual zero-dimensional (0D) discrete-time model (May, 1974; Reluga, 2004) with the aim of deriving the simplest model that represents the fundamental physics occurring at the boundary between vegetated and bare areas (Paola & Leeder, 2011). By considering a control volume approach applied to the entire length of the vegetated area (L_v) (Supporting Information, Fig. S6A), we obtain a simplified description of the erosion and uprooting processes that occur at the boundary between the vegetated and bare areas. Riverbed erosion (E) results from the imbalance between bedload flux entering (q_B^{IN}) and leaving (q_B^{OUT}) the control volume in a given interval of time (ΔT) and is obtained by applying Eq. 1 in discrete form:

$$E = \Delta z_B = \frac{q_B^{IN} - q_B^{OUT}}{L_v} \Delta t. \quad (3)$$

In the control volume, the initial slope S is assumed to be constant over time, and the Shields stress used to calculate the entering and leaving bedload fluxes is calculated assuming a wide and rectangular cross-section and uniform flow conditions. It leads, with

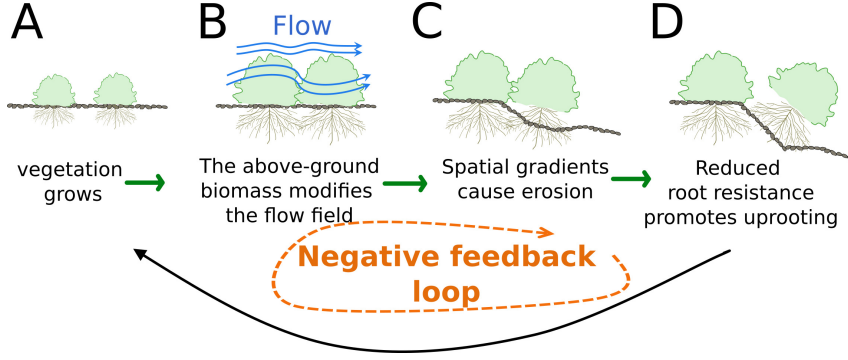


Figure 1. Schematic representation of the biogeomorphic negative feedback loop. Vegetation grows (A) and increases the roughness, resulting in reduced flow velocity within the vegetated area (B). Vegetation reduces sediment transport, leading to a greater imbalance between the vegetated and bare areas and thus inducing erosion (C). Erosion increases the likelihood of vegetation uprooting, and when scour reaches root depth, uprooting occurs (D). The overall feedback loop is negative: higher vegetation biomass causes greater sediment flux imbalance and more erosion, ultimately resulting in less vegetation. Vegetation regrows during low-flow periods, maintaining the negative feedback cycle.

these assumptions, to:

$$\theta = \left(\frac{q}{ks} \right)^{\frac{3}{5}} \frac{S_{10}^{\frac{7}{10}}}{(s-1)d_s}, \quad (4)$$

where s is the sediment relative density (set to 2.65). The roughness coefficient in the vegetated area and the bedload flux leaving the control volume are computed with the same equation as in the 1D model. In this case, the sediment balance is computed as $(q_B^{IN} - q_B^{OUT}) = (\gamma^{\frac{10}{3}} - 1)q_B^{OUT}$, which is always negative as $\gamma < 1$. Then, the model follows the same workflow as the 1D model (Supporting Information, Fig. S2) and retains the same biogeomorphic feedbacks and logistic law of vegetation growth.

The main challenge in deriving the 0D model is the description of the uprooting mechanism. We assume that the uprooting process depends on the ratio between disturbance and resistance \mathcal{W} following the jump condition $B^- = \mathcal{U}(\mathcal{W})B^+$. The uprooting function $\mathcal{U}(\mathcal{W})$ characterizes the survival of vegetation during floods and exhibits two limiting behaviors. When erosion is negligible and uprooting does not occur (i.e. $\mathcal{W} \rightarrow 0$), $\mathcal{U} \rightarrow 1$. Conversely, when erosion removes all vegetation (i.e. $\mathcal{W} \rightarrow \infty$), $\mathcal{U} \rightarrow 0$. To investigate the behavior of the uprooting function between these limiting cases, we performed numerical simulations using the 1D model. First, we used a specific configuration that closely resembled the conditions of the 0D model. This approach lumped biomass into a single value, ignoring the spatial distribution of vegetation within the patch (see Supporting Information, Fig. S4A and S4C). Next, we run the 1D model with a standard setting to determine the effects of the spatial distribution of vegetation on the uprooting function. Our analysis yielded the following uprooting function (Supporting Information, Fig. S7A and Fig. S7B):

$$\mathcal{U}(\mathcal{W}) = \begin{cases} 1 & \text{if } 0 \leq \mathcal{W} < w_m, \\ \left(1 - \frac{\mathcal{W} - w_m}{1 - w_m} \right)^\beta & \text{if } w_m \leq \mathcal{W} \leq 1, \\ 0 & \text{if } \mathcal{W} > 1. \end{cases} \quad (5)$$

$\beta \geq 1$ is a nonlinear shape parameter and larger values indicate that even weak erosion can lead to a significant decrease in biomass. Meanwhile, w_m is a threshold parameter, representing the minimum value of \mathcal{W} for uprooting to occur. These two parameters were obtained by fitting Equation 5 to the results obtained with the 1D model in its full setting (Supporting Information, Fig. S7C). Remarkably, results consistently demonstrated that β frequently exceeded unity, with a maximum value of 9, while w_m ranged from 0 to 0.4 (Supporting Information, Fig. S7C).

By combining Eq.(3) and Eq.(2) with Eq.(5), we obtain the following difference equation:

$$B_{n+1}^- = \begin{cases} B_{n+1}^+ & \text{if } 0 \leq \mathcal{W}_{n+1} < w_m, \\ \left(1 - \frac{\mathcal{W}_{n+1} - w_m}{1 - w_m}\right)^\beta B_{n+1}^+ & \text{if } w_m \leq \mathcal{W}_{n+1} \leq 1, \\ B_{min} & \text{if } \mathcal{W}_{n+1} > 1, \end{cases} \quad (6)$$

Here we have:

$$\mathcal{W}_{n+1} = \frac{E_p(B_{n+1}^+)}{\zeta_{upr}}, \quad B_{n+1}^+ = \frac{B_n^- K e^{\sigma \Delta T_F}}{B_n^- (e^{\sigma \Delta T_F} - 1) + K} \quad (7)$$

$$E_p(B_{n+1}^+) = \left\{ C_2 - C_1 [\max(\Theta - \theta_{cr}, 0)]^{\frac{3}{2}} \right\} \frac{\Delta T_F}{L_v}, \quad (8)$$

with

$$C_1 = \frac{8\sqrt{(s-1)gd_s^3}}{1-p}, \quad C_2 = C_1 (\theta_g - \theta_{cr})^{\frac{3}{2}}, \quad C_3 = \frac{q^{3/5}S}{ks_g^2(s-1)d_s}, \quad (9)$$

and

$$\Theta = C_3 \left[\left(\frac{ks_v - ks_g}{K} \right) B_{n+1}^+ + ks_g \right]^{\frac{7}{5}}. \quad (10)$$

To establish morphodynamic equivalence between the full 1D model and the 0D model, we calibrated the flood duration and reduced it such that $T_F(0D)/T_F(1D) = 0.26$, ensuring that the average erosion in the control volume matches the erosion potential E_p of the 1D model. By numerically solving the discrete model with this adjusted flood duration, we obtained the graphs motivating Eq. (6). These graphs exhibit nonlinear parabolic behavior, with the maximum value depending on the parameters σ , β , and w_m (Supporting Information, Figs. S6B and S6C).

3 Results

3.1 Nonlinear Dynamics Characteristics

Dynamical systems analysis is used to study the asymptotic behavior of the time series of the variables of the 1D model. Results are presented in terms of average vegetation biomass. The same dynamics are observed for the other two variables, i.e. bed elevation and water depth. Simulation results show that our 1D model predicts three possible behaviors: i) constant biomass equal to carrying capacity (Fig. 2A); ii) periodic changes between two (as in Fig. 2B) or more (but finite) values; iii) aperiodic chaotic fluctuations bounded by a chaotic attractor (Fig. 2C). The first behavior is observed when vegetation grows slowly, erosion is weak, and thus no uprooting occurs. Although the vegetation grows over time, the associated erosion at the boundary between the vegetated

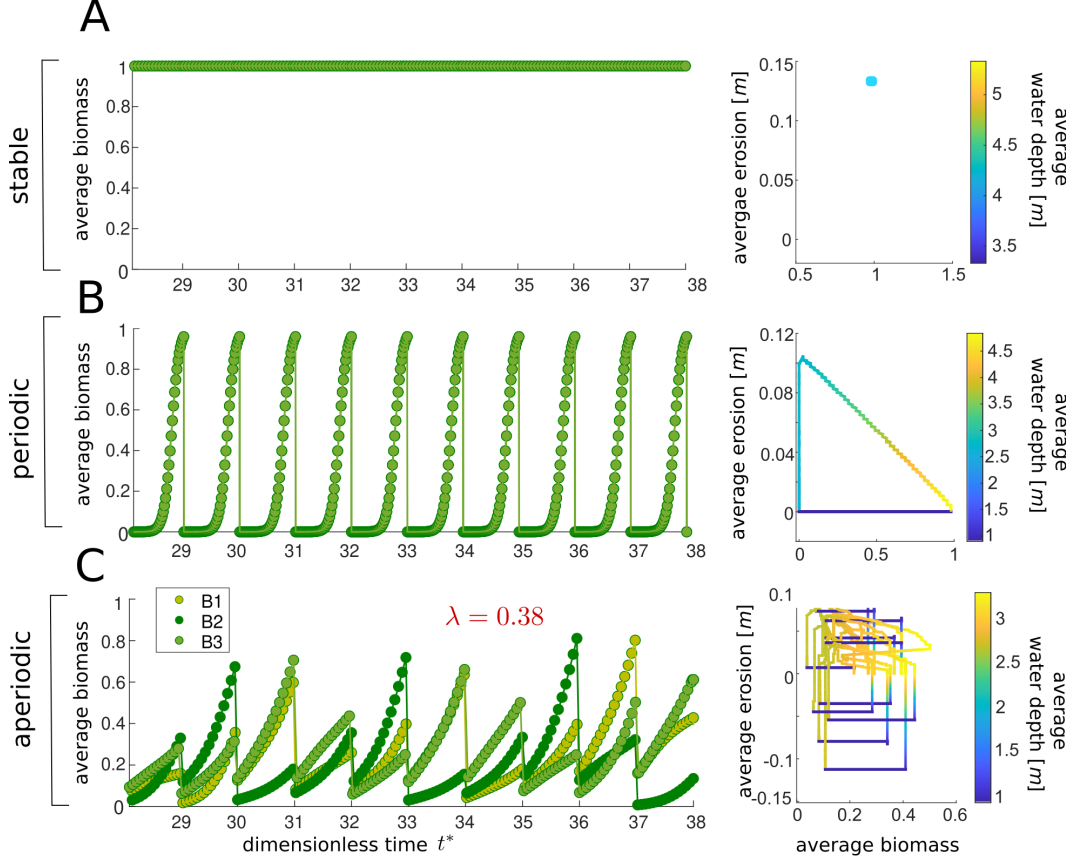


Figure 2. Average vegetation biomass over time (*left*) and in phase space (*right*) obtained by the 1D model. Three different behaviors are possible: (A) stable, (B) periodic, and (C) aperiodic dynamics. The parameters used are: (A) $\sigma = 0.2$, $\mathcal{W}_{z_B} = 1.0 \times 10^{-3}$, (B) $\sigma = 0.8$ and $\mathcal{W}_{z_B} = 2.9$, (C) $\sigma = 0.2$, $\mathcal{W}_{z_B} = 2.9$. Results from three independent model runs with nearly identical initial vegetation distributions (B1= 1.0×10^{-5} , B2= 1.1×10^{-5} , B3= 1.2×10^{-5}) show the sensitivity of the solution to the initial conditions. The Lyapunov coefficient is given for the chaotic case for the runs with initial vegetation distribution B1.

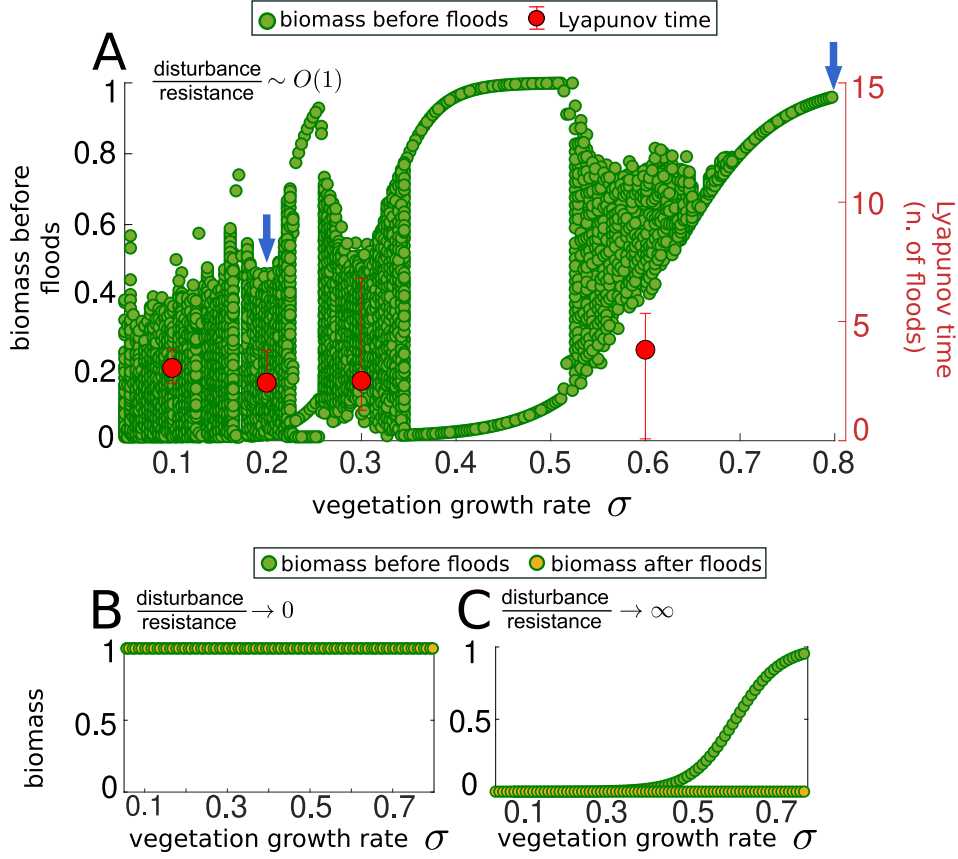


Figure 3. Bifurcation diagrams obtained by the 1D model for different values of the ratio between disturbance and resistance \mathcal{W}_{zB} : (A) $\mathcal{W}_{zB} = 2.9$, chaotic dynamics is widespread; (B) $\mathcal{W}_{zB} = 1.0 \times 10^{-3}$, vegetation grows to its carrying capacity and remains constant over time; (C) $\mathcal{W}_{zB} = 1.0 \times 10^6$, vegetation is completely removed during floods, resulting in a bare bed after each flood. Biomass before the flood depends on the growth rate σ , and can be close to 0 for very low growth rates or 1 for $\sigma = 1$. Blue arrows in (A) mark the conditions reported in (Fig. 2B and 2C)

area and the bare riverbed never reaches the root depth. Thus, the vegetation is free to grow until it reaches the carrying capacity and remains constant over time. The trajectory of the vegetated area in phase space, defined by the averaged values of biomass (x -axis), bed elevation change (y -axis) and water depth (color scale), is a distinct point when the initial growth-flood cycles are neglected and the focus is on the asymptotic behavior (Right Fig. 2A). Periodic dynamics occurs when vegetation biomass grows to a constant value during a single growth-flood cycle and is completely or partially uprooted during the following flood. It can take up to three growth-flood cycles for the vegetation to reach a critical biomass that causes significant erosion, leading to biomass removal. The corresponding attractor in phase space is an invariant loop (Right Fig. 2B). When the dynamics is chaotic, the vegetation biomass fluctuates, never repeating exactly the same cycles, although the state of the system in phase space is constrained to a chaotic attractor (Right Fig. 2C). Typically, vegetation that develops during low-flow periods is partially removed by subsequent floods. In some cases, however, complete removal of vegetation may occur.

“Deterministic chaos” is defined not only by aperiodic fluctuations, but also by sensitivity to initial conditions (Strogatz, 2018; Turchin, 2013). To test this, we perform three independent model runs for each configuration, starting from nearly identical initial vegetation distributions. The results show that stable or periodic trajectories are insensitive to initial conditions and almost indistinguishable (Fig. 2A and 2B). On the contrary, when the solution is aperiodic, the three model runs diverge in time, confirming the chaotic behavior (Fig. 2C). Furthermore, the three trajectories were used to compute the maximum Lyapunov exponent (λ), as a measure of the divergence of the infinitesimally close trajectories. We used previously published algorithms (Rosenstein et al., 1993; Kantz, 1994) that directly tests for exponential divergence of close trajectories (see Supporting Information Text 1). As known from dynamical systems theory, positive values of the Lyapunov exponent are characteristic of a chaotic system with aperiodic fluctuations (Supporting Information, Fig. S5). In this case, a relevant parameter is the Lyapunov time, defined as the inverse of the Lyapunov exponent and representing the characteristic timescale at which a chaotic system becomes unpredictable. For stable or periodic configurations with trajectories of initially close points that do not diverge, the Lyapunov exponents are negative; the system is predictable and the Lyapunov time $\rightarrow \infty$.

To generate a bifurcation diagram, we plot the asymptotic biomass versus vegetation growth rate; it shows how changes in this parameter affect biomass dynamics (Fig. 3A). Within the range of $[0.0, 0.65]$, solid bands are caused by chaos, and open areas are the result of periodic cycles. A stable period-3 cycle is found in the range $[0.22, 0.26]$, and a stable period-2 cycle is observed in the largest periodic window in the σ -range $[0.34, 0.52]$. For growth rates above 0.69, biomass grows and eventually reaches a periodic orbit. In the chaotic region we consistently found positive values of the maximum Lyapunov exponent. The corresponding Lyapunov time is always equal to only a few (2-4) growth-flood cycles (Fig. 3A, red dots and right vertical axis).

Our model exhibits chaotic behavior only when the flood disturbance (and the associated erosion) is of the same order of magnitude as the vegetation resistance (the root depth). When \mathcal{W}_{z_B} is much smaller than 1, the resistance dominates and the vegetation always reaches the steady state at the carrying capacity (Fig. 3B). In contrast, when \mathcal{W}_{z_B} is much larger than 1, the disturbance dominates and the vegetation is completely uprooted during the flood (Fig. 3C). In both these limiting cases, chaos is prevented.

3.2 Route to Chaos and Predictability Horizon

While we find compelling evidence for the existence of chaos, the 1D model does not elucidate the mechanisms for the onset of chaos. The bifurcation diagram in Fig. (3A) does not clearly show a definitive route to chaos. This lack of clarity is mainly due to the uneven spatial variation in biomass distribution and bed erosion within the vegetated area. Therefore, we used the 0D model and analyzed the resulting bifurcation diagram which reveals a clear period-doubling path to chaos (Fig. 4A). The first and second bifurcations occur at about $\sigma = 0.102$ and $\sigma = 0.127$, respectively, and the chaotic regime starts at about $\sigma = 0.134$. The corresponding maximum Lyapunov exponents are negative when the solution is periodic, zero at the bifurcation points, and positive when the system behaves chaotically (Fig. 4B). In this case, the Lyapunov time is about 2 growth-flood cycles ($\lambda \approx 0.5$), confirming a very short predictability horizon as computed with the 1D model. Despite the further simplification and removal of the spatial component, the 0D model shows a dynamic behavior similar to that of the 1D model, indicating that the biogeomorphic feedbacks and the intrinsic disturbance mechanism are the key ingredients generating the chaotic behavior.

Our results show that the Lyapunov exponent is approximately independent of the model parameters and remains constant when the ratio of disturbance to resistance \mathcal{W} is of order one (Fig. 4C). Chaotic behavior is prevented when \mathcal{W} tends to zero or infin-

ity (Fig. 4C, *Inset*), resulting in negative Lyapunov exponents. In addition, we examine the variability of the Lyapunov exponent as a function of the unit-width gravel, computed as the product of the unit-width discharge (q) by the river slope, S , in a range typical of gravel-bed rivers (Fig. 4D). Again, the values are largely constant, between 0.4 and 0.7, and depend more on the choice of parameters β and w_m than on the values of the stream power. However, rivers with small stream power (0.02-0.03 m^2/s) are characterized by smaller values of the Lyapunov exponents and thus longer predictability horizon.

4 Discussion and Implication

Our study reveals that the intrinsic nonlinear feedbacks between vegetation, flow and sediment transport can generate deterministic chaos, thus fundamentally limiting the predictability of the temporal evolution of the system. The results of the proposed models indicate that when chaos occurs, the maximum Lyapunov time is short and can be quantified by a few (2 to 4) vegetation growth-flood cycles. In natural rivers, the duration of these growth-flood cycles can vary considerably, depending on the type of vegetation (e.g., aquatic vs. riparian) and on the flood magnitude that is able to uproot the vegetation. In low-energy small rivers where macrophytes are the main engineering species (Gurnell, 2014) the growth-flood cycle is likely to be annual. In larger gravel-bed rivers, the return interval of floods that can significantly affect vegetation has been reported to vary from 1-2 years for partial vegetation removal on highly dynamic braided rivers (Surian et al., 2015), to several decades for major vegetation renewal (Belletti et al., 2014). Riparian trees grow rapidly, exerting a strong impact on the flow field already after a few years, when the biomass is closer to the ground. Also the resistance of riparian plants develops in short time, where roots of phreatophytic plants grow to reach the ground water level and can easily reach depths $> 1m$ in 1-2 years (Mahoney & Rood, 1998). Our analysis suggests that chaotic behavior is more likely to manifest when the magnitude of flood disturbance and associated erosion closely matches the resistance exerted by the roots. Therefore, different river systems may exhibit chaotic behavior on different time scales, also depending on the growth stage of the vegetation and its root network. Moreover, our results suggest that external factors that amplify the erosion process, such as bedform migration and bank erosion, are likely to modify the nonlinear dynamics considered here, where the morphological disturbance is uniquely generated by the presence of vegetation. Increased erosion, if not balanced by vegetation resistance, may prevent the emergence of chaos within the system. This intrinsic mechanism is not limited to rivers and can play an important role in different types of vegetated landscapes, where the interplay between time-dependent disturbances and vegetation resistance is key to shaping their evolution, such as in salt marshes, wetlands, and coastal dunes (Goldstein & Moore, 2016; Marani et al., 2010; Bertagni et al., 2018; Schwarz et al., 2018).

Chaotic behavior has been found in fluvial system considering only sediment-flow interactions, when flow is redistributed in multiple anabranches, like in braided rivers (Stecca & Hicks, 2022) and in deltas (Salter et al., 2020). However, in less complex river morphologies, such as those with migrating bars, the emergence of chaos from these interactions remains unproven (Schielen et al., 1993), although it may occur within certain parameter ranges. Our results demonstrate that adding vegetation may enhance the occurrence of deterministic chaos. On the other hand, additional processes, such as flow stochasticity that has a strong control on vegetation dynamics (Bertagni et al., 2018), may add further complexity to the system and can either enhance or mitigate the chaotic behavior resulting from the interactions of flow, sediment, and vegetation. Our modelling approach was not intended to fully characterize a specific river system, but to show that the main intrinsic feedback between vegetation growth and flow disturbance is likely to generate chaos.

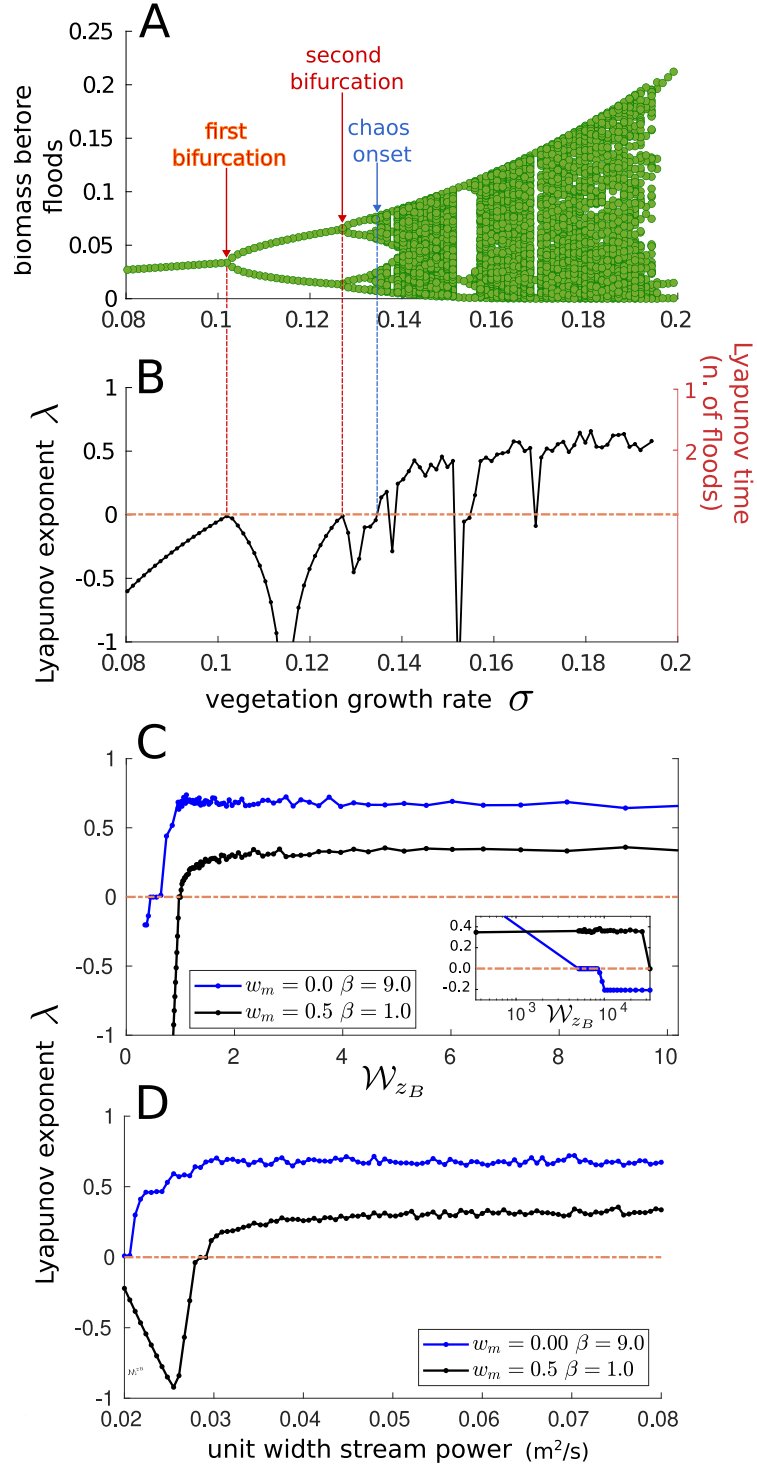


Figure 4. (A) Bifurcation diagram showing total biomass as a function of the vegetation growth rate for the 0D model: the onset of chaos is achieved by classical period doubling. (B) Corresponding plot of Lyapunov exponent. (C) The maximum Lyapunov exponent is positive and nearly constant over a wide range of disturbance/resistance ratios, and (D) also for typical ranges of unit-width stream power.

Despite chaotic systems' inherent unpredictability, it is still possible and relevant to use numerical models to quantify their statistical behavior, e.g., by using ensemble methods. These methods, commonly used in weather forecasting, involve the generation of multiple realizations of the model (Bauer et al., 2015). By using an ensemble approach, we can analyze and predict the behavior of vegetated rivers while using observational data to reduce uncertainty.

5 Data Availability Statement

The 1D and 0D Matlab codes along with all the Matlab codes used to generate Figures 2, 3, and 4 are openly available at <https://doi.org/10.5281/zenodo.10426969>.

Acknowledgments

We are grateful to Michele Castelluzzo for conducting preliminary analysis on the computation of the maximum Lyapunov exponent.

References

- Bankhead, N. L., Thomas, R. E., & Simon, A. (2017). A combined field, laboratory and numerical study of the forces applied to, and the potential for removal of, bar top vegetation in a braided river. *Earth Surface Processes and Landforms*, 42(3), 439–459. doi: 10.1002/esp.3997
- Bau', V., Borthwick, A. G., & Perona, P. (2021). Plant roots steer resilience to perturbation of river floodplains. *Geophysical Research Letters*, 48(9), e2021GL092388.
- Bauer, P., Thorpe, A., & Brunet, G. (2015). The quiet revolution of numerical weather prediction. *Nature*, 525(7567), 47–55.
- Belletti, B., Dufour, S., & Piégay, H. (2014). Regional assessment of the multi-decadal changes in braided riverscapes following large floods (example of 12 reaches in south east of france). *Advances in Geosciences*, 37, 57–71. Retrieved from <https://adgeo.copernicus.org/articles/37/57/2013/> doi: 10.5194/adgeo-37-57-2014
- Bertagni, M., Camporeale, C., & Perona, P. (2018). Parametric transitions between bare and vegetated states in water-driven patterns. *Proceedings of the National Academy of Sciences*. doi: 10.1073/pnas.1721765115
- Bertoldi, W., Siviglia, A., Tettamanti, S., Toffolon, M., Vetsch, D., & Francalanci, S. (2014). Modeling vegetation controls on fluvial morphological trajectories. *Geophysical Research Letters*, 41(20), 7167–7175. Retrieved from <http://dx.doi.org/10.1002/2014GL061666> doi: 10.1002/2014GL061666
- Bouma, T., Van Duren, L., Temmerman, S., Claverie, T., Blanco-Garcia, A., Ysebaert, T., & Herman, P. (2007). Spatial flow and sedimentation patterns within patches of epibenthic structures: Combining field, flume and modelling experiments. *Continental Shelf Research*, 27(8), 1020–1045.
- Braudrick, C. A., Dietrich, W. E., Leverich, G. T., & Sklar, L. S. (2009). Experimental evidence for the conditions necessary to sustain meandering in coarse-bedded rivers. *Proceedings of the National Academy of Sciences*, 106(40), 16936–16941.
- Bywater-Reyes, S., Wilcox, A. C., Stella, J. C., & Lightbody, A. F. (2015). Flow and scour constraints on uprooting of pioneer woody seedlings. *Water Resources Research*, 51(11), 9190–9206.
- Caponi, F., & Siviglia, A. (2018). Numerical modeling of plant root controls on gravel bed river morphodynamics. *Geophysical Research Letters*, 45(17), 9013–9023.

- Caponi, F., Vetsch, D. F., & Siviglia, A. (2020). A model study of the combined effect of above and below ground plant traits on the ecomorphodynamics of gravel bars. *Scientific reports*, 10(1), 1–14.
- Corenblit, D., Baas, A. C. W., Bornette, G., Darrozes, J., Delmotte, S., Francis, R. A., ... Steiger, J. (2011). Feedbacks between geomorphology and biota controlling Earth surface processes and landforms: A review of foundation concepts and current understandings. *Earth-Science Reviews*, 106(3–4), 307–331. Retrieved from <http://www.sciencedirect.com/science/article/pii/S0012825211000377> doi: <http://dx.doi.org/10.1016/j.earscirev.2011.03.002>
- Corenblit, D., Tabacchi, E., Steiger, J., & Gurnell, A. M. (2007). Reciprocal interactions and adjustments between fluvial landforms and vegetation dynamics in river corridors: a review of complementary approaches. *Earth-Science Reviews*, 84(1–2), 56–86.
- D’Alpaos, A., Toffolon, M., & Camporeale, C. (2016). Ecogeomorphological feedbacks of water fluxes, sediment transport and vegetation dynamics in rivers and estuaries. *Advances in Water Resources*, 93, 151–155.
- Diehl, R. M., Wilcox, A. C., Stella, J. C., Kui, L., Sklar, L. S., & Lightbody, A. (2017). Fluvial sediment supply and pioneer woody seedlings as a control on bar-surface topography. *Earth Surface Processes and Landforms*, 42(5), 724–734. doi: 10.1002/esp.4017
- Edmaier, K., Burlando, P., & Perona, P. (2011). Mechanisms of vegetation uprooting by flow in alluvial non-cohesive sediment. *Hydrology and Earth System Sciences*, 15(5), 1615–1627. doi: 10.5194/hess-15-1615-2011
- Follett, E. M., & Nepf, H. M. (2012). Sediment patterns near a model patch of reedy emergent vegetation. *Geomorphology*, 179, 141–151.
- Goldstein, E. B., & Moore, L. J. (2016). Stability and bistability in a one-dimensional model of coastal foredune height. *Journal of Geophysical Research: Earth Surface*, 121(5), 964–977.
- Gurnell, A. M. (2014). Plants as river system engineers. *Earth Surface Processes and Landforms*, 39(1), 4–25.
- Gurnell, A. M., Petts, G. E., Hannah, D. M., Smith, B. P., Edwards, P. J., Kollmann, J., ... Tockner, K. (2001). Riparian vegetation and island formation along the gravel-bed fiume tagliamento, Italy. *Earth Surface Processes and Landforms: The Journal of the British Geomorphological Research Group*, 26(1), 31–62.
- Jourdain, C., Claude, N., Tassi, P., Cordier, F., & Antoine, G. (2020). Morphodynamics of alternate bars in the presence of riparian vegetation. *Earth Surface Processes and Landforms*, 45(5), 1100–1122.
- Kantz, H. (1994). A robust method to estimate the maximal lyapunov exponent of a time series. *Phys. Lett. A*, 185, 77.
- Kim, H. S., Kimura, I., & Shimizu, Y. (2015). Bed morphological changes around a finite patch of vegetation. *Earth Surface Processes and Landforms*, 40(3), 375–388. Retrieved from <http://dx.doi.org/10.1002/esp.3639> (ESP-13-0354.R3) doi: 10.1002/esp.3639
- Le Bouteiller, C., & Venditti, J. G. (2014). Vegetation-driven morphodynamic adjustments of a sand bed. *Geophysical Research Letters*, 41(11), 3876–3883. doi: 10.1002/2014GL060155
- Le Bouteiller, C., & Venditti, J. (2015). Sediment transport and shear stress partitioning in a vegetated flow. *Water Resources Research*, 51(4), 2901–2922.
- Mahoney, J. M., & Rood, S. B. (1998, 12). Streamflow requirements for cottonwood seedling recruitment—an integrative model. *Wetlands*, 18, 634–645. Retrieved from <https://link.springer.com/10.1007/BF03161678> doi: 10.1007/BF03161678
- Marani, M., D’Alpaos, A., Lanzoni, S., Carniello, L., & Rinaldo, A. (2010). The importance of being coupled: Stable states and catastrophic shifts in tidal

- biomorphodynamics. *Journal of Geophysical Research: Earth Surface*, 115(F4).
- May, R. M. (1974). Biological populations with nonoverlapping generations: stable points, stable cycles, and chaos. *Science*, 186(4164), 645–647.
- Meyer-Peter, E., & Müller, R. (1948). Formulas for bed-load transport. In *2nd meeting, int. assoc. of hydraul. eng. and res.* Stockholm.
- Murray, A., Knaapen, M., Tal, M., & Kirwan, M. (2008). Biomorphodynamics: Physical-biological feedbacks that shape landscapes. *Water Resources Research*, 44(11).
- Nardin, W., & Edmonds, D. A. (2014). Optimum vegetation height and density for inorganic sedimentation in deltaic marshes. *Nature Geoscience*, 7(10), 722.
- Nepf, H. M. (2012). Flow and Transport in Regions with Aquatic Vegetation. *Annual Review of Fluid Mechanics*, 44(1), 123–142. Retrieved from <http://dx.doi.org/10.1146/annurev-fluid-120710-101048> doi: 10.1146/annurev-fluid-120710-101048
- Palmer, M., & Ruhi, A. (2019). Linkages between flow regime, biota, and ecosystem processes: Implications for river restoration. *Science*, 365(6459), eaaw2087.
- Paola, C., & Leeder, M. (2011). Simplicity versus complexity. *Nature*, 469(7328), 38–39.
- Parker, G. (2004). The quasi-steady approximation, chap. 13. *1D Sediment Transport Morphodynamics with Applications to Rivers and Turbidity Currents..* (http://hydrolab.illinois.edu/people/parkerg/powerpoint_lectures.htm)
- Pasquale, N., Perona, P., Francis, R., & Burlando, P. (2012). Effects of stream-flow variability on the vertical root density distribution of willow cutting experiments. *Ecological Engineering*, 40, 167–172. Retrieved from <http://dx.doi.org/10.1016/j.ecoleng.2011.12.002> doi: 10.1016/j.ecoleng.2011.12.002
- Perona, P., & Crouzy, B. (2018, 2). Resilience of riverbed vegetation to uprooting by flow. *Proceedings of the Royal Society A: Mathematical, Physical and Engineering Sciences*.
- Phillips, J. D. (2003). Sources of nonlinearity and complexity in geomorphic systems. *Progress in physical geography*, 27(1), 1–23.
- Reinhardt, L., Jerolmack, D., Cardinale, B. J., Vanacker, V., & Wright, J. (2010). Dynamic interactions of life and its landscape: feedbacks at the interface of geomorphology and ecology. *Earth Surface Processes and Landforms*, 35(1), 78–101.
- Reluga, T. C. (2004). Analysis of periodic growth–disturbance models. *Theoretical population biology*, 66(2), 151–161.
- Rosenstein, M. T., Collins, J. J., & De Luca, C. J. (1993). A practical method for calculating largest lyapunov exponents from small data sets. *Physica D: Nonlinear Phenomena*, 65(1-2), 117–134.
- Salter, G., Voller, V. R., & Paola, C. (2020). Chaos in a simple model of a delta network. *Proceedings of the National Academy of Sciences*, 117(44), 27179–27187.
- Scheffer, M., Carpenter, S., Foley, J. A., Folke, C., & Walker, B. (2001). Catastrophic shifts in ecosystems. *Nature*, 413(6856), 591–596.
- Schielen, R., Doelman, A., & De Swart, H. (1993). On the nonlinear dynamics of free bars in straight channels. *Journal of Fluid Mechanics*, 252, 325–356.
- Schwarz, C., Gourgue, O., Van Belzen, J., Zhu, Z., Bouma, T. J., Van De Koppel, J., ... Temmerman, S. (2018). Self-organization of a biogeomorphic landscape controlled by plant life-history traits. *Nature Geoscience*, 11(9), 672–677.
- Stecca, G., & Hicks, D. M. (2022). Numerical simulations of confined braided river morphodynamics: Display of deterministic chaos and characterization through turbulence theory. *Journal of Geophysical Research: Earth Surface*, 127(3),

- e2021JF006409.
- Strogatz, S. H. (2018). *Nonlinear dynamics and chaos: with applications to physics, biology, chemistry, and engineering*. CRC press.
- Surian, N., Barban, M., Ziliani, L., Monegato, G., Bertoldi, W., & Comiti, F. (2015). Vegetation turnover in a braided river: frequency and effectiveness of floods of different magnitude. *Earth Surface Processes and Landforms*, 40(4), 542–558. Retrieved from <https://onlinelibrary.wiley.com/doi/abs/10.1002/esp.3660> doi: <https://doi.org/10.1002/esp.3660>
- Tal, M., & Paola, C. (2007). Dynamic single-thread channels maintained by the interaction of flow and vegetation. *Geology*, 35(4), 347–350.
- Temmerman, S., Bouma, T., Van de Koppel, J., Van der Wal, D., De Vries, M., & Herman, P. (2007). Vegetation causes channel erosion in a tidal landscape. *Geology*, 35(7), 631. Retrieved from <http://dx.doi.org/10.1130/G23502A.1> doi: 10.1130/G23502A.1
- Turchin, P. (2013). Complex population dynamics. In *Complex population dynamics*. Princeton university press.
- Wang, C., & Temmerman, S. (2013). Does biogeomorphic feedback lead to abrupt shifts between alternative landscape states?: An empirical study on intertidal flats and marshes. *Journal of Geophysical Research: Earth Surface*, 118(1), 229–240. Retrieved from <https://agupubs.onlinelibrary.wiley.com/doi/abs/10.1029/2012JF002474> doi: 10.1029/2012JF002474
- Wang, C., Wang, Q., Meire, D., Ma, W., Wu, C., Meng, Z., ... Temmerman, S. (2016). Biogeomorphic feedback between plant growth and flooding causes alternative stable states in an experimental floodplain. *Advances in Water Resources*, 93, 223–235. Retrieved from <https://www.sciencedirect.com/science/article/pii/S0309170815001505> doi: <https://doi.org/10.1016/j.advwatres.2015.07.003>
- Wohl, E., Lane, S. N., & Wilcox, A. C. (2015). The science and practice of river restoration. *Water Resources Research*, 51(8), 5974–5997.
- Yager, E., & Schmeeckle, M. (2013). The influence of vegetation on turbulence and bed load transport. *Journal of Geophysical Research: Earth Surface*, 118(3), 1585–1601.
- Zong, L., & Nepf, H. (2012). Vortex development behind a finite porous obstruction in a channel. *Journal of Fluid Mechanics*, 691, 368–391. doi: 10.1017/jfm.2011.479

River ecomorphodynamic models exhibit features of nonlinear dynamics and chaos

I. Cunico¹, W. Bertoldi¹, F. Caponi², H. A. Dijkstra³, A. Siviglia¹

¹Department of Civil, Environmental and Mechanical Engineering, University of Trento, Italy

²Laboratory of Hydraulics, Hydrology and Glaciology (VAW), ETH Zurich, Zurich, Switzerland

³Institute for Marine and Atmospheric Research Utrecht, Utrecht University, Utrecht, The Netherlands

Contents of this file

1. Text S1
2. Table S1
3. Figures S1 to S8

Introduction The Supporting Information provides detailed descriptions of the methods used in the manuscript, complementing the main text. It also includes a table of the model run parameters and eight figures referenced in the main text.

Corresponding author: I.Cunico, (ilaria.cunico@unitn.it)

December 20, 2023, 7:00pm

1. 1D model: Numerical solution and simulations

The numerical solution is obtained by solving the Exner (Eq. 2 in the main text) by using a Godunov method (Toro, 2001), while the water surface profile is obtained by directly solving the gradually varied flow equation using a standard solver for ordinary differential equations. The numerical domain consists of 200 equally spaced cells. Initial conditions are obtained by setting uniform flow conditions at both the inlet and outlet of the numerical domain and running a fixed-bed simulation until steady state is reached. We then perform morphodynamic simulations, keeping z_B fixed at both the inlet and the outlet. We ran the code for 500 growth-flood cycles for the 1D model. We excluded the first 300 cycles to ensure that transient behavior did not affect the analysis of the remaining 200 cycles. Similarly, for the 0D model, we ran the code for 1000 growth-flood cycles, discarding the first 700 cycles to account for any transient behavior before analyzing the remaining 300 cycles.

2. Calculation of the Maximum Lyapunov exponent

We used the largest Lyapunov exponent (λ) to quantify the exponential separation of initially close trajectories and to characterize the dynamic behavior of the biomass time series obtained with the 1D model. Consider two trajectories that are initially separated by a distance $\delta_0 \ll 1$, where $\delta_{\Delta t}$ is the distance between them at time Δt . Then λ is given by $\delta_{\Delta t} \simeq \delta_0 \exp(\lambda t)$ with $\delta_{\Delta t} \ll 1$ and $\Delta t \gg 1$. Positive Lyapunov exponents indicate exponential divergence of nearby trajectories, i.e. chaotic dynamics, which dictates the time scale (Lyapunov time= $1/\lambda$) for accurate predictions. Conversely, negative Lyapunov exponents dictate the time scale for the decay of perturbations of the system. Calculations

were performed with the TISEAN 3.0.1 software package, using the *lyap_k* program (Hegger et al., 1999). Data points from the initial transient phase of the simulations (growth-flood cycle 1-50) have been omitted from both analyses and graphs. The magnitude of the largest Lyapunov exponent was estimated from the divergence curve, which represents the average rate of divergence of neighboring points in the attractor as a function of time. We estimated the maximum Lyapunov exponent from the slope of a straight line fitted to the linear part of the ln-transformed divergence of the time series data. Positive estimates of the Lyapunov exponent indicate chaos-like irregular dynamics, whereas negative values indicate stable or periodic solutions (Kantz, 1994; Rosenstein et al., 1993). For the 0D discrete model, we calculated the Lyapunov exponent using the method described in Section 10.5 of (Strogatz, 2018).

References

- Hegger, R., Kantz, H., & Schreiber, T. (1999). Practical implementation of nonlinear time series methods: The tisean package. *Chaos: An Interdisciplinary Journal of Nonlinear Science*, 9(2), 413–435.
- Kantz, H. (1994). A robust method to estimate the maximal lyapunov exponent of a time series. *Phys. Lett. A*, 185, 77.
- Meyer-Peter, E., & Müller, R. (1948). Formulas for bed-load transport. In *2nd meeting, int. assoc. of hydraul. eng. and res.* Stockholm.
- Rosenstein, M. T., Collins, J. J., & De Luca, C. J. (1993). A practical method for calculating largest lyapunov exponents from small data sets. *Physica D: Nonlinear Phenomena*, 65(1-2), 117–134.

Table S1. Model run parameters

Parameter	Description	Value
L	Channel length	1500 m
S	Channel slope	0.006
x_{up}	Upstream coordinate of the vegetation patch	600 m
x_{dw}	Downstream coordinate of the vegetation patch	900 m
L_v	Vegetation patch length	300 m
q	Constant flood unit width discharge	$12 \text{ m}^2/\text{s}$
M	Number of numerical cells	200
p	Porosity	0.4
ds	Sediment diameter	6 cm
q_B	Unit width sediment flux	calculated with (Meyer-Peter et al., 1948)
ks_g	Strickler coefficient of the bare riverbed	$30 \text{ m}^{1/3}\text{s}^{-1}$
ks_v	Minimum Strickler coefficient with vegetation	$8 \text{ m}^{1/3}\text{s}^{-1}$
σ	Vegetation growth rate	[0-1]
K	Carrying capacity	1
B_{min}	Initial vegetation biomass	1.0×10^{-5}
E_p	Erosion potential	0.35 m
ζ_{upr}	Uprooting depth	12 cm
T_v	Vegetation growth time scale	1 growing season (1 year)
T_F	Flood duration in the 1D model	3 h
ΔT_F	Time interval between floods	T_v
$T_F(0D)$	Flood duration in the 0D model	0.78 h

Strogatz, S. H. (2018). *Nonlinear dynamics and chaos: with applications to physics, biology, chemistry, and engineering*. CRC press.

Toro, E. F. (2001). *Shock-capturing methods for free-surface shallow flows*. Wiley-Blackwell.

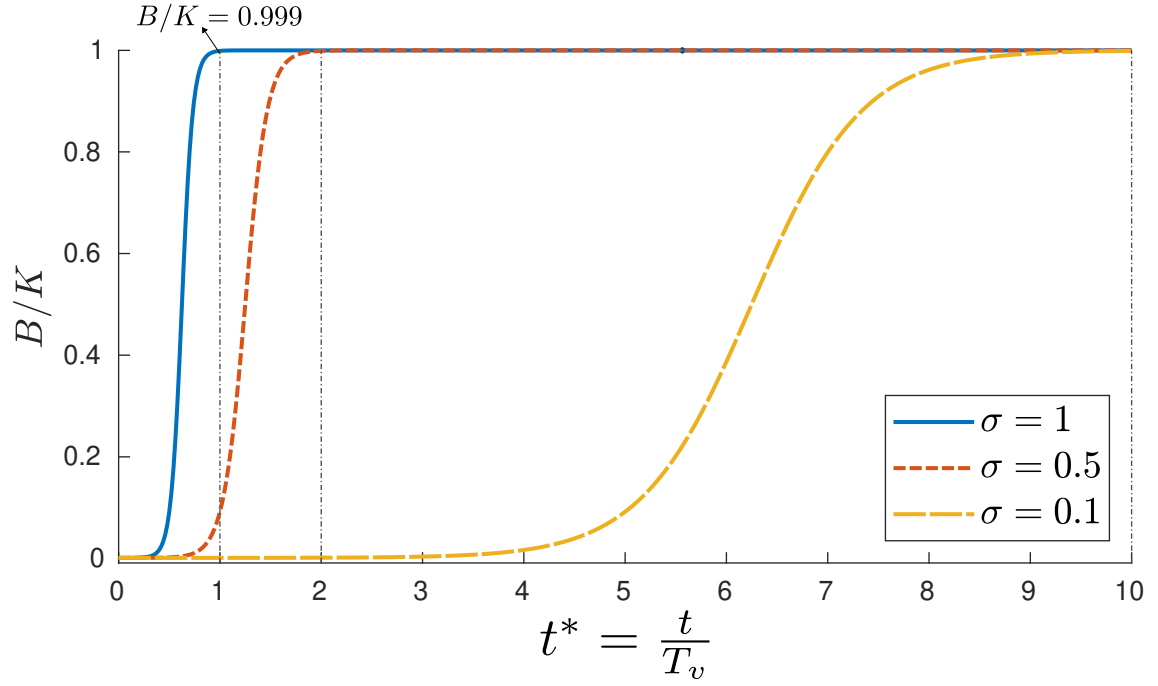


Figure S1. Logistic growth. Different types of vegetation are characterized by different growth rates σ . A vegetation with $\sigma = 1$ reaches the 99.9% of maximum growth (i.e., $B/K = 0.999$) at $t = T_v$. A vegetation with $\sigma = 0.1$ reaches $B/K = 0.999$ at $t = 10T_v$. In general, the smaller the σ , the slower the growth. We use the scale T_v to define the dimensionless time $t^* = t/T_v$.

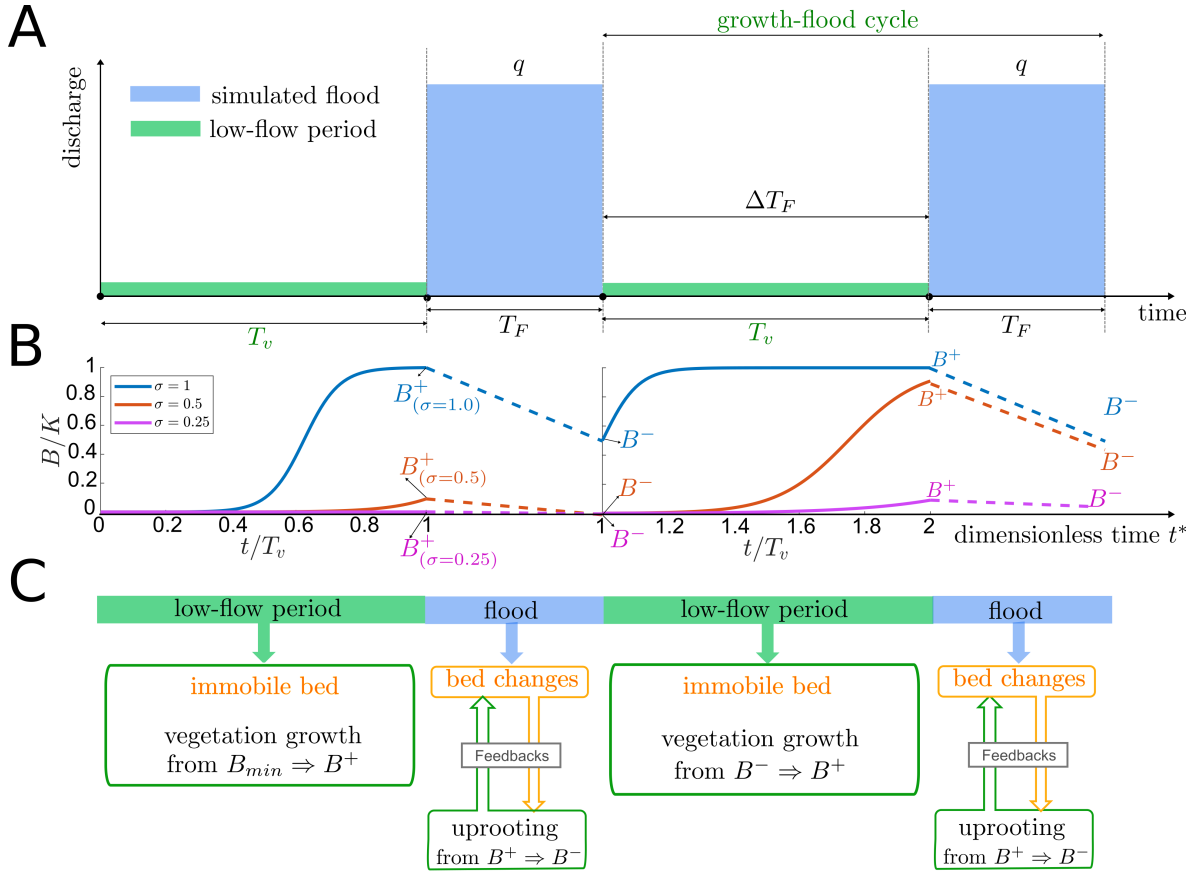


Figure S2. Schematic illustration of the ecomorphodynamic model functioning. An alternating sequence of growth-flood cycles is considered, with floods having a duration of T_F and being followed by low-flow periods of T_v . The time interval between two successive floods is ΔT_F . Since T_F (hours, days) $\ll T_v$ (months, years), the duration of the flood T_F and the growing period T_v are not to scale. (B) and (C), the growth of vegetation is deterministic and follows the logistic law. In this work, we assume that $\Delta T_F = T_v$, i.e., that vegetation with $\sigma = 1$ reaches the 99.9% of carrying capacity between two successive floods, regardless of its initial value (blue lines). In general, biomass B increases from its initial value (B^-) to its final value (B^+) during low-flow period. During the flood, the discharge is assumed to be constant and the Shields stress is above the critical value, which may cause changes in the riverbed. This can uproot vegetation, transitioning biomass from B^+ before the flood to B^- after the flood. For a given value of σ , the surviving biomass B^- is used as the initial condition in the logistic growth equation during the following growth period.

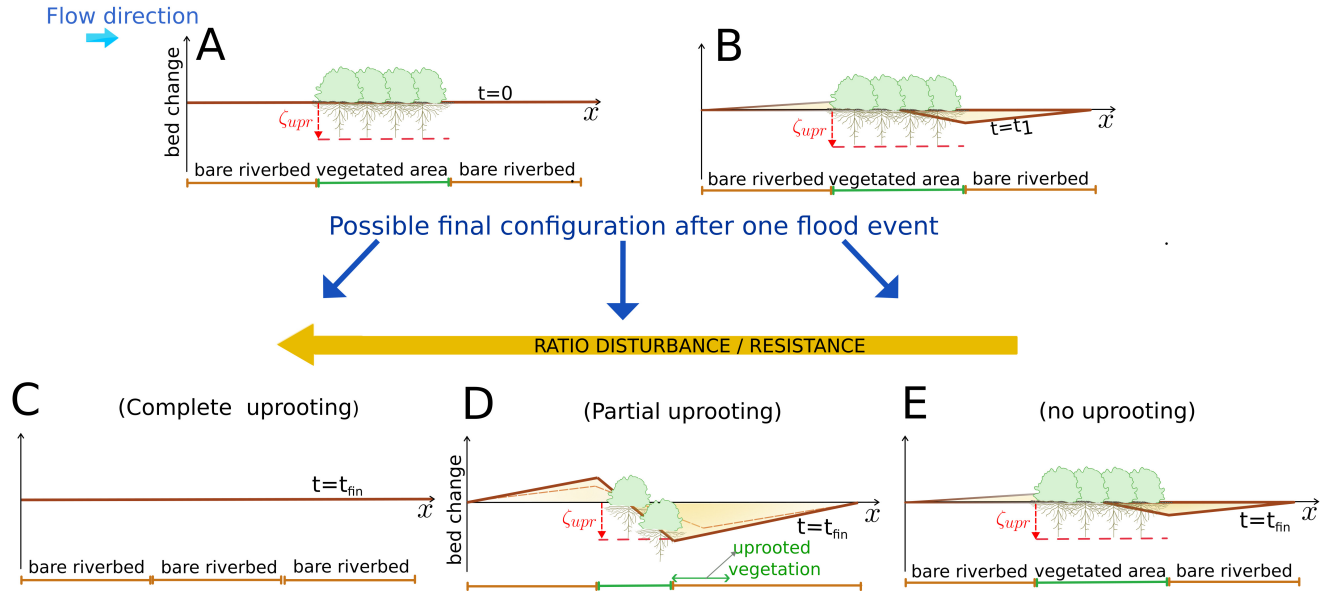


Figure S3. Riverbed evolution of a straight gravel channel with a vegetated area. (A) Schematic illustration of the initial condition ($t = 0$) and (B) and time evolution of the riverbed ($t = t_1$), evaluated in terms of bed level changes ($z_B(x, t) - z_B(x, t = 0)$). Sediment erosion occurs at the downstream end. The final configuration ($t = t_{fin}$) after a flood event is determined by the ratio of disturbance to resistance. When this ratio is high, vegetation is completely uprooted (C), allowing the riverbed to return to its original configuration. As the ratio decreases, vegetation may be either partially uprooted (D) or not uprooted at all (E). The slope within the vegetated area is adjusted to maintain sediment balance in these last two scenarios.

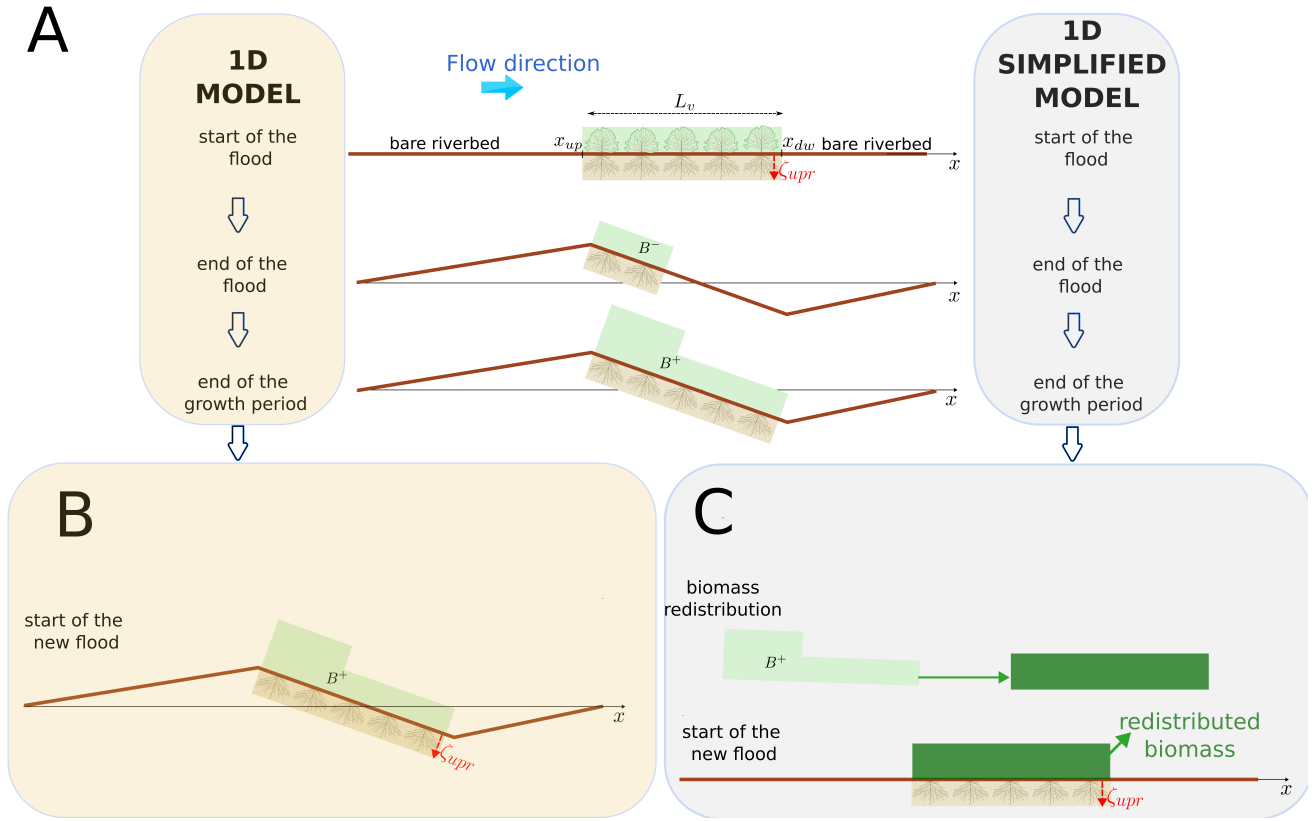


Figure S4. Schematic illustration of the 1D ecomorphodynamic model (A and B) and its simplified version (A and C). (A) In both models, before the first flood, the bed has a constant slope S , the vegetation biomass is evenly distributed in the vegetated area, and the rooting depth is ζ_{upr} . After the flood the vegetation is partially removed and the slope in the vegetated area has changed. Vegetation regrows during the low flow period, resulting in an uneven distribution of biomass at the end of the growth period. Biomass is higher where it has not been removed. The rooting depth is set at ζ_{upr} . (B) This corresponds to the initial condition for the next flood for the 1D model. (C) The simplified version of the 1D model includes a uniform redistribution of biomass in the patch (preserving the total biomass) and resets the bed to the initial value S and the rooting depth to ζ_{upr} .

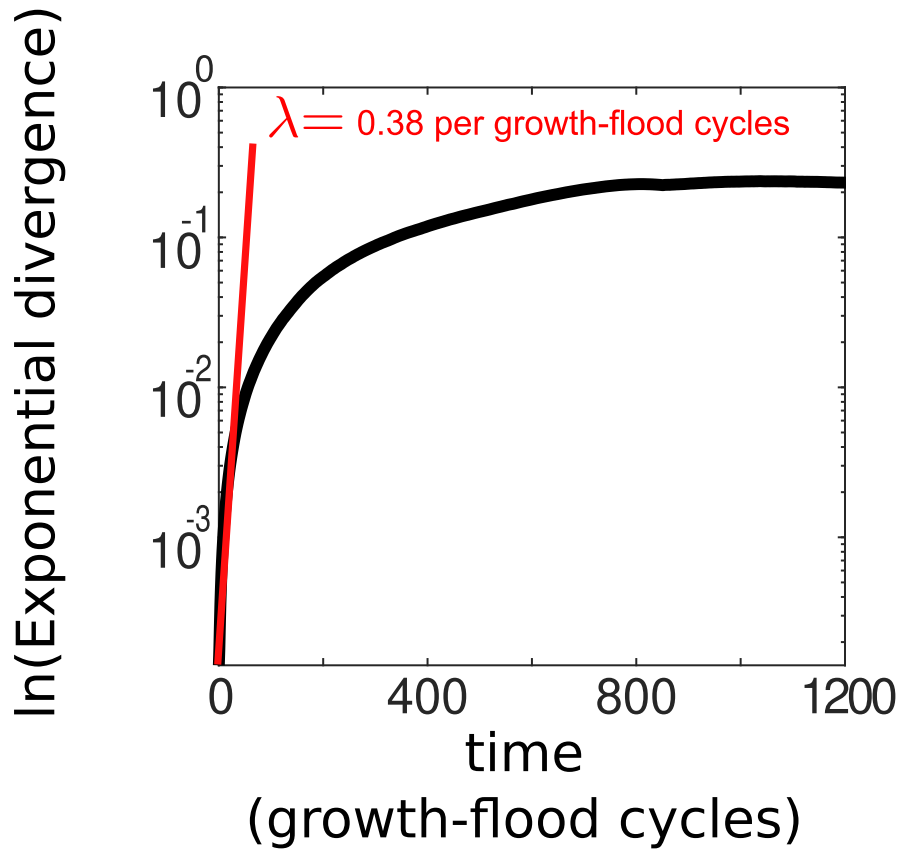


Figure S5. Exponential divergence of the trajectories. When the dynamics are aperiodic (Fig. 2C in the main text), the Lyapunov exponent is positive, indicating the presence of chaos-like irregular dynamics. The Lyapunov exponent (λ) is calculated as the initial slope of the ln-transformed exponential divergence versus time, as estimated by linear regression (red line).

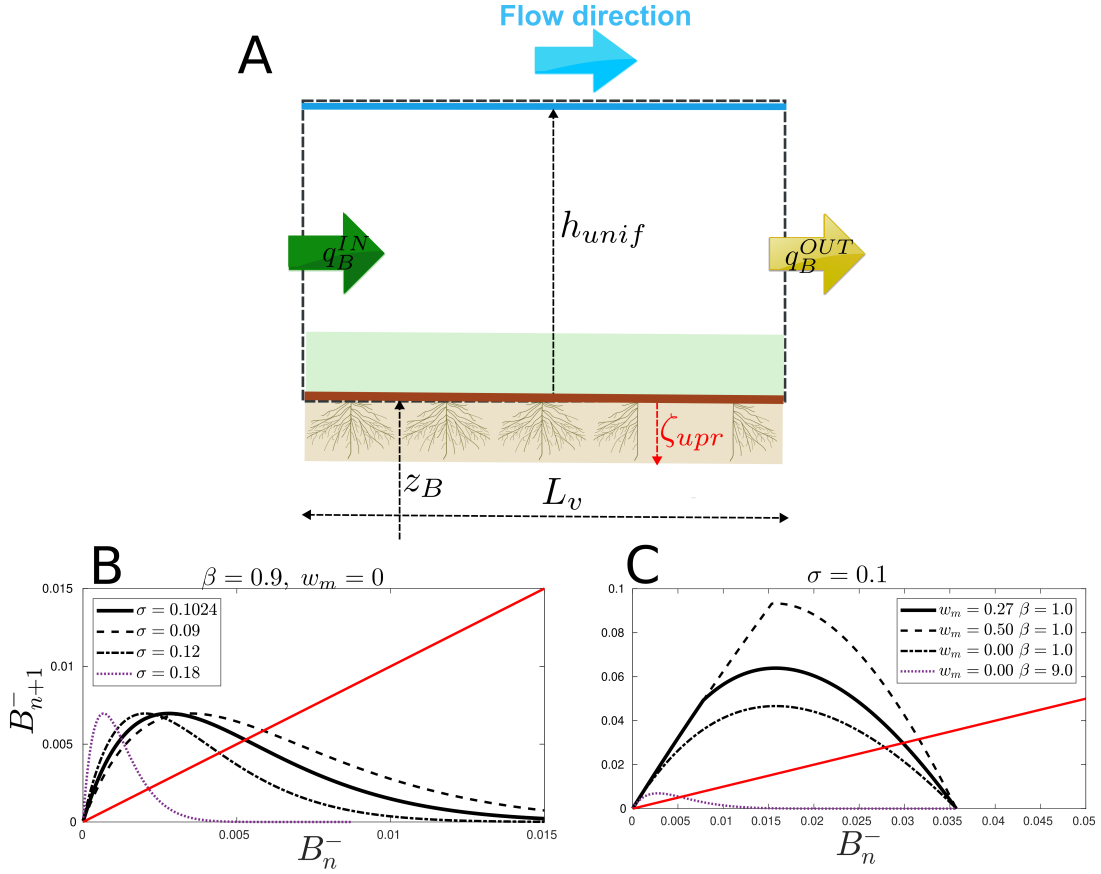


Figure S6. (A) The 0D discrete model is derived using a control volume that spans the entire vegetated area length L_v . Assumptions of this model include a constant initial slope S , a wide and rectangular cross section, and calculation of water depth h_{unif} based on uniform flow conditions. Erosion occurs within the control volume when the bedload flux entering the volume q_B^{IN} exceeds the bedload flux leaving the volume q_B^{OUT} . The rooting depth in the control volume is assumed to be constant and equal to ζ_{upr} . (B and C) The solutions of the difference equation for the 0D model (Eq. 6 in the main text) show a parabolic behavior with a maximum value that depends on the parameters used. The red line in the figure represents the diagonal line $B_{n+1}^- = B_n^-$. The position of the fixed points can be determined by calculating the intersection of the parabolas with the diagonal line. If the derivative of the discrete equation calculated at the fixed point is ≤ -1 , then the fixed point is unstable and leads to periodic solutions. These solution are obtained using the parameters given in Table S1.

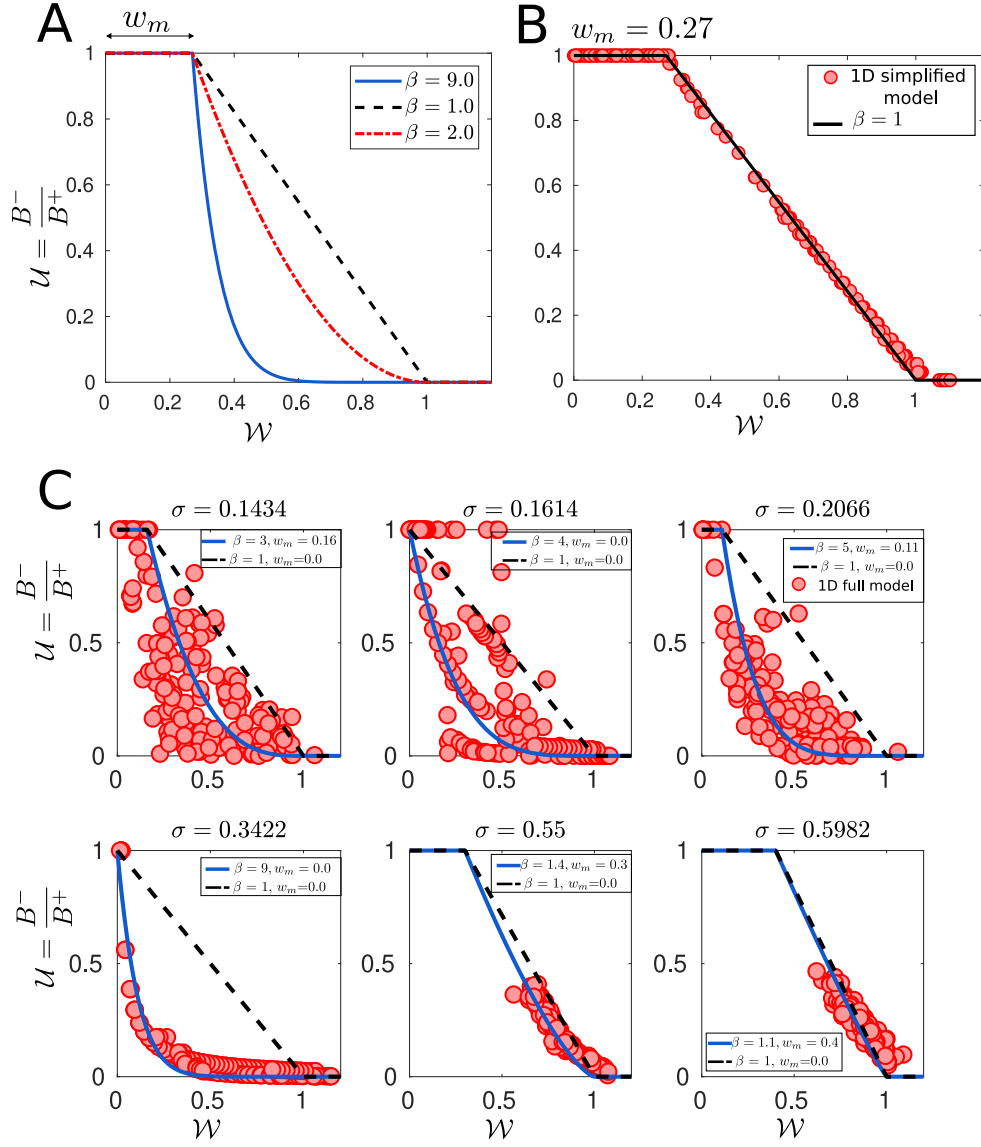


Figure S7. (A) Behavior of the uprooting function $U(W)$, which characterizes the survival of vegetation during floods. The function exhibits two limiting behaviors, i.e. when erosion is negligible and uprooting does not occur (i.e. $W \rightarrow 0$), then $U \rightarrow 1$. Conversely, when erosion removes all vegetation (i.e. $W > 1$), then $U \rightarrow 0$. The uprooting function resulting from simulations performed with the 1D simplified model exhibits a linear behavior with $\beta = 1$ and $w_m = 0.27$ (B), The uprooting function resulting from simulations performed with the 1D model in its full setting exhibits a strong nonlinear behavior (C), which can be approximately fit using $\beta > 1$ and w_m varying roughly between 0 and 0.4. All simulations in this figure has been carried out with the parameters given in Table S1.

December 20, 2023, 7:00pm